Journal of Magnetism and Magnetic Materials 604 (2024) 172288

Contents lists available at ScienceDirect

Journal of Magnetism and Magnetic Materials

journal homepage: www.elsevier.com/locate/jmmm

Research article

Control of magnetism on the topological SnTe(001) surface by doping, strain, and gap opening

Bui D. Hoi [a,*], Doan Q. Khoa [b], Nguyen T. Dung [c], Ho Viet [d], Vo T. Lam [e]

[a] Faculty of Physics, University of Education, Hue University, Hue 530000, Viet Nam
[b] The University of Danang - University of Science and Technology, Da Nang 550000, Viet Nam
[c] School of Engineering and Technology, Vinh University, 182 Le Duan street, Vinh City, Nghe An province, Viet Nam
[d] Department of Research Management and International Relations, Hue Industrial College, Hue 530000, Viet Nam
[e] Faculty of Natural Sciences Pedagogy, Sai Gon University, 273 An Duong Vuong Str., District 5, Ho Chi Minh City, Viet Nam

ARTICLE INFO

Keywords:
Topological surface
Green's function
Doping
Electric field
Strain
(Anti)ferromagnetic spin–spin interaction

ABSTRACT

The spin–spin exchange interaction is an important observable that helps in understanding the magnetism of materials. Topological materials are of particular interest due to their strong spin–orbit coupling, which makes them promising for applications in valleytronics and spintronics. In this study, we have theoretically demonstrated the ability to control the switching of ferromagnetic (FM) and antiferromagnetic (AFM) couplings between two magnetic impurities on the (001) surface of the topological crystalline insulator SnTe. By considering experimental parameters such as doping, strain, and gap opening at surface Dirac cones, we provide a generic way to build the FM-AFM and clockwise–counterclockwise phase diagrams of SnTe(001), which are still missing in the literature, especially for the spintronics community.

1. Introduction

spin–spin exchange interaction on the surface or in the bulk of a material [1–3] is important for spintronic applications [4,5]. One specific type of such interaction is the indirect Ruderman–Kittel–Kasuya–Yosida (RKKY) coupling between two classical magnetic impurities doped on a conductor [6–8], which strongly depends on the behavior of electrons of the host material [9]. Magnetic moments of the doped impurities form ferromagnetic (FM) and antiferromagnetic (AFM) couplings. RKKY coupling oscillates between FM and AFM [10–15] phases with increasing the distance between impurities.

A new class of materials, so-called topological insulators, have introduced a new phase where insulating and metallic phases coexist in the bulk and on the surface, respectively. Their bulk states are gapped, while their surface states are gapless. Additionally, these materials have strong spin–orbit coupling due to the presence of heavy atoms. A notable characteristic of topological insulators is their time-reversal symmetry [16–19], which adds to their unique properties and is responsible for protecting the gapless surface states. However, there exist considerable topological materials such as weak topological insulators [20–23] and topological crystalline insulators (TCIs) [24–29] in which the gapless surface states are additionally protected by the crystal symmetries. Unlike topological insulators, TCIs have an even number of gapless states. This property makes them potentially useful for transport applications in both valleytronics and spintronics.

Controlling the electronic properties is an effective way to tune the physical properties of systems. This is because other degrees of freedom can be easily affected through a connection to the charge degree of freedom. As an example, the anisotropic ferroelectric distortion has been shown to modulate the RKKY interaction on the SnTe(001) surface, which is a well-known TCI. This modulation can switch the FM and AFM couplings [30]. Moreover, research has also shown that a weak Floquet optical driving can form a noncollinear twisted RKKY interaction on the doped SnTe(001) surface [31].

It is crucial to control magnetic orders in topological materials for spintronics applications such as magnetic data storage devices [32]. In this study, we have successfully achieved the switching of FM and/or AFM coupling of magnetic impurities on the surface of TCIs through the implementation of doping (due to the presence of an electron or hole bath), strain (due to mechanical stress or pressure), and gap (due to substrate effects, electrical gating, nanoscale sculpturing, etc.). It is important to note that the term "gap" refers to the energy gap (or band gap) that can appear at the Dirac point on the surface. This approach provides new and valuable physical and practical insights that have not been explored before.

This paper is structured into four sections. In Section 2, the Hamiltonian model of the pristine and strain- and gap-induced SnTe(001) surface is presented, and the RKKY interaction is calculated in the

* Corresponding author.
E-mail address: buidinhhoi@hueuni.edu.vn (B.D. Hoi).

https://doi.org/10.1016/j.jmmm.2024.172288
Received 24 May 2024; Received in revised form 18 June 2024; Accepted 25 June 2024
Available online 29 June 2024

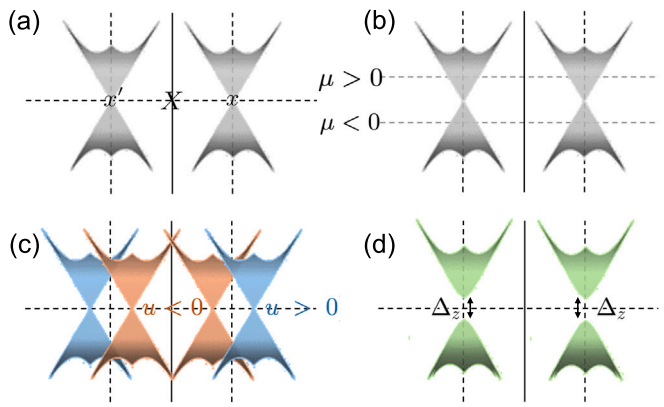

Fig. 1. (a) The pristine Dirac cone in the low-energy limit around the X point of the SnTe(001) surface is located at the x and x' points. (b) When doped, the Dirac cone undergoes changes in its electronic properties. (c) When strained, the Dirac cone is displaced. (d) When gapped, the Dirac cone's electronic properties and carrier density can be modified.

presence of doping, strain, and gap opening. Section 3 presents the results for switching between FM and AFM couplings. Finally, the paper is summarized in Section 4.

2. Theoretical background

In this section, we present a continuum model for the Dirac fermions (gapless states) on the SnTe(001) surface [26–29,33,34]. The model is constructed using p orbitals of sublattices Sn and Te, and spin–orbitally coupled states $|1\rangle = (|\downarrow, \mathrm{Sn}\rangle + |\uparrow, \mathrm{Te}\rangle)/\sqrt{2}$ and $|2\rangle = (|\uparrow, \mathrm{Sn}\rangle + |\downarrow, \mathrm{Te}\rangle)/\sqrt{2}$. The ground states are formed by two spin–orbitally coupled coaxial Dirac cones, which are separated in the low-energy limit, see Fig. 1(a). These cones, located around the X point on the projected Brillouin zone (BZ) of SnTe(001) surface, are denoted as $x = \sqrt{n^2+\delta^2}/v_x$ and $x' = -\sqrt{n^2+\delta^2}/v_x$ [30,33–36]. The Fermi velocity along the x-direction is found to be $v_x = 3.53$ eV.Å [35,37], while the intervalley scattering parameters are $n = 0.055$ eV and $\delta = 0.04$ eV [33,35,35,37]. There are also two Dirac cones (not shown here), y and y', located around the Y point with a Fermi velocity of $v_y = 1.91$ eV.Å. To obtain the Hamiltonians of the y and y' Dirac cones around the Y point on the SnTe(001) surface, C_4 symmetry should be applied on the X point.

Let us focus on the non-pristine states. We start with the effects of doping on the system. When we add or remove electrons from a solid, the band structure is affected, and the Fermi level shifts accordingly. This change in energy level is known as the chemical potential (μ), see Fig. 1(b). We can incorporate the effects of doping by including it in our model's Fermi energy, which will affect the RKKY couplings.

In the case of the strain effect, the orbital degrees of freedom are modulated as the main origins of the electronic properties in solids [38, 39]. It is achieved by shifting the momentum space due to a lattice displacement $\vec{u}$ with components $u_{\ell\ell'} = (\partial_\ell u_{\ell'} + \partial_{\ell'} u_\ell)/2$ (we neglect the shear terms u_{xy} and u_{yx} as an approximation) along the $\{\ell, \ell'\} \in \{x, y\}$ direction. To analyze the strain effect in the momentum space, a gauge field vector potential $\vec{A} = \tilde{x} - x$ is employed, where $\tilde{x}$ represents the strained Dirac cone, as illustrated in Fig. 1(c). This results in $\vec{A} = (c_1 u_{xx} + c_2 u_{yy}, c_1 u_{yy} + c_2 u_{xx})$ [40], where strained momenta (compared to the pristine ones (k_x, k_y)) are given by $\tilde{k}_x = k_x + c_1 u_{xx} + c_2 u_{yy}$ and $\tilde{k}_y = k_y + c_1 u_{yy} + c_2 u_{xx}$; $c_1 = 0.3\text{∀}^{-1}$ and $c_2 = 1.4\text{∀}^{-1}$ refer to orbital nature of the strained electronic bands [38].

In the case of the gap effect, we employ a universal description of various effects such as substrate effects, electrical gating, and nanoscale sculpturing to open a band gap Δ_z at each Dirac cone, see Fig. 1(d).

Eventually, the strained and gapped Hamiltonian reads

$$H_{x/x'}(\tilde{k}, \Delta_z) = \tilde{v}_x(\tilde{k}_x \mp x)\sigma_y - v_y \tilde{k}_y \sigma_x + \tfrac{\Delta_z}{2}\sigma_z\,, \tag{1}$$

where $\tilde{v}_x = \delta/x$ [35] and $\{\sigma_x, \sigma_y\}$ are the sublattice Pauli matrices. In what follows, we neglect the weak anisotropicity in the Hamiltonian and use $\tilde{v}_x = v_y = v_F \simeq 2$ eV.Å.

Now, we consider two magnetic impurities ($\vec{S}_1$:= moment, $\vec{R}_1$:= position) and ($\vec{S}_2$, $\vec{R}_2$) on the SnTe(001) surface [6–8]. Also, we consider the host itinerant electron $\vec{s}$. The interaction Hamiltonian between magnetic impurities and the itinerant electron is given by $H_{\mathrm{int}} = \mathcal{J}\sum_{i=1}^{2} \vec{S}_i \cdot \vec{s}_i$, where $\mathcal{J}$ is the bare exchange interaction. Assuming $\vec{R} = \vec{R}_2 - \vec{R}_1$ as the impurity separation, the second-order perturbation theory gives rise to the following RKKY Hamiltonian

$$H^{\alpha\beta}_{\mathrm{RKKY}}(\vec{R}) = \mathcal{J}^2 \sum_{\ell,\ell'} S_1^{\ell\,\alpha}\, \chi^{\alpha\beta}_{\ell\ell'}(\vec{R})\, S_2^{\ell'\,\beta}\,, \tag{2}$$

where α and β refer to the sublattices Sn and Te and $\{\ell, \ell'\} = \{x, y, z\}$. Importantly, $\chi^{\alpha\beta}_{\ell\ell'}(\vec{R})$ depicts the spin susceptibility, which can be calculated from the retarded Green's functions in the spin space [11–13,41]:

$$\chi^{\alpha\beta}_{\ell\ell'}(\vec{R}) = -\frac{2}{\pi}\,\Im \int_{-\infty}^{E_F} dE\, \eta^{\alpha\beta}_{\ell\ell'}(E, \vec{R})\,, \tag{3}$$

where $\eta^{\alpha\beta}_{\ell\ell'}(E, \vec{R}) = \mathrm{Tr}\,[\sigma_\ell\, G_{\alpha\beta}(E, \vec{R})\, \sigma_{\ell'}\, G_{\beta\alpha}(E, -\vec{R})]$ and $E_F = \mu$ is the Fermi energy and/or the chemical potential at zero temperature. The presence of spin–orbit coupling on the SnTe(001) surface has a significant impact on the retarded Green's functions, which results in the spin contribution of sublattices. This consequently implies that every element of the Green's function is non-zero. In contrast, without spin–orbit coupling, the off-diagonal terms vanish. This finding is crucial in understanding the behavior of Dirac materials and can lead to significant advancements in the field of spintronics. Therefore,

$$G_{\alpha\beta}(E, \vec{R}) = \begin{pmatrix} G^{\uparrow\uparrow}_{\alpha\beta}(E, \vec{R}) & G^{\uparrow\downarrow}_{\alpha\beta}(E, \vec{R}) \\ G^{\downarrow\uparrow}_{\alpha\beta}(E, \vec{R}) & G^{\downarrow\downarrow}_{\alpha\beta}(E, \vec{R}) \end{pmatrix}. \tag{4}$$

To cover the entire BZ of the surface with an area of Ω_{SBZ} and enable cross-talk between all the Dirac cones, it is necessary to consider all directions. Thus,

$$\begin{aligned} G^{ss'}_{\alpha\beta}(E, \vec{R}) = \frac{1}{\Omega_{\mathrm{SBZ}}} \int d^2\tilde{k}\, e^{i\vec{\tilde{k}}\cdot\vec{R}} \Big[\, & e^{i\vec{X}\cdot\vec{R}} G^{ss'}_{\alpha\beta}(\vec{\tilde{k}} + \vec{X}, E) \\ & + e^{i\vec{Y}\cdot\vec{R}} G^{ss'}_{\alpha\beta}(\vec{\tilde{k}} + \vec{Y}, E) \Big]\,, \end{aligned} \tag{5}$$

where $\{s, s'\} = \{\uparrow, \downarrow\}$. Rewriting the above equation results in $G^{ss'}_{\alpha\beta}(E, \vec{R}) = e^{iX R_x}\left(e^{ix R_x}\mathcal{Y}^{ss'}_{\alpha\beta}(E, \vec{R}) + e^{-ix R_x}\underline{\mathcal{Y}}^{ss'}_{\alpha\beta}(E, \vec{R})\right) + e^{iY R_y}\left(e^{iy R_y}\mathcal{W}^{ss'}_{\alpha\beta}(E, \vec{R}) + e^{-iy R_y}\underline{\mathcal{W}}^{ss'}_{\alpha\beta}(E, \vec{R})\right)$, where $R_x = R\cos(\varphi_R)$ and $R_y = R\sin(\varphi_R)$ with φ_R being the direction between two impurities. By defining $E + io^+ = i\varepsilon$ for $o^+ \ll 1$, we make use of the relation

$$\mathcal{Y}^{ss'}_{\alpha\beta}(\varepsilon, \vec{R}) = \frac{1}{\Omega_{\mathrm{SBZ}}} \int_0^\infty \tilde{k}\, d\tilde{k} \int_0^{2\pi} d\varphi_{\tilde{k}}\, e^{i\tilde{k}\,R\cos(\varphi_{\tilde{k}} - \varphi_R)}\, \mathcal{Y}^{ss'}_{\alpha\beta}(\tilde{k}, \varepsilon)\,, \tag{6}$$

where $\varphi_{\tilde{k}} = \tan^{-1}(\tilde{k}_y/\tilde{k}_x)$ and we have $\mathcal{Y}^{ss'}_{x/x'}(\tilde{k}, \varepsilon) = 1/[i\varepsilon - H_{x/x'}(\tilde{k}, \Delta_z)]$ around the X point. Incorporating the strain effect into the angle between two impurities through the phase factor in Eq. (6) is an interesting scenario, resulting in $\tilde{\varphi}_R = \varphi_R + \theta_u$, where $\theta_u = \tan^{-1}(A_y/A_x)$ with $A_x = c_1 u_{xx} + c_2 u_{yy}$ and $A_y = c_1 u_{yy} + c_2 u_{xx}$.

Thereby, the Green's functions for the x and x' Dirac cones are based on hybrid states $|1\rangle$ and $|2\rangle$ [31] read

$$\mathcal{Y}_{11(22)}(\varepsilon, \vec{R}) = -C\left(i\varepsilon + (-)^{\frac{\Delta_z}{2}}\right) K_0(\tilde{\varepsilon}\, R/v_F)\,, \tag{7a}$$

$$\mathcal{Y}_{12(21)}(\varepsilon, \vec{R}) = -(+)\, C\, \tilde{\varepsilon}\, e^{-(+)i\tilde{\varphi}_R}\, K_1(\tilde{\varepsilon}\, R/v_F)\,, \tag{7b}$$

where $C = 2\pi/\Omega_{\mathrm{SBZ}}\, v_F^2$, $\tilde{\varepsilon} = \sqrt{(\varepsilon - i\mu)^2 + \Delta_z^2/4}$, and $K_{0/1}$ is the modified Bessel function. As for the Dirac cones around the Y point, similar

expressions can be obtained following the C_4 symmetry. The following relations are valid between $\mathcal{V}$s: $\mathcal{V}_{11/22}(\varepsilon,-\vec{R}) = \mathcal{V}_{11/22}(\varepsilon,\vec{R})$ and $\mathcal{V}_{12/21}(\varepsilon,-\vec{R}) = -\mathcal{V}_{12/21}(\varepsilon,\vec{R})$. Finally, we obtain

$$H^{\alpha\alpha,\nu}_{\mathrm{RKKY}}(\vec{R}) = \sum_{\ell} J_{\ell}(\vec{R}) S^{\ell}_1 S^{\ell}_2 + \nu J_{\mathrm{s},xy}(\vec{R})[S^x_1 S^y_2 + S^y_1 S^x_2] + \vec{J}^{\,\nu}_{\mathrm{as}} \cdot (\vec{S}_1 \times \vec{S}_2), \tag{8a}$$

$$H^{\alpha\beta,\tau}_{\mathrm{RKKY}}(\vec{R}) = J_x(\vec{R}) S^x_1 S^x_2 - J_y(\vec{R}) S^y_1 S^y_2 - J_z(\vec{R}) S^z_1 S^z_2 + \vec{J}^{\,\tau}_{\mathrm{as}} \cdot (\vec{S}_1 \times \vec{S}_2), \tag{8b}$$

where $\nu = +1$ (-1) and $\tau = +1$ (-1) refers to the TeTe (SnSn) and TeSn (SnTe) sublattices, respectively, and

$$\vec{J}^{\,\nu}_{\mathrm{as}} = (J_{\mathrm{as},x}, \nu J_{\mathrm{as},y}, 0), \tag{9a}$$

$$\vec{J}^{\,\tau}_{\mathrm{as}} = (-J_{\mathrm{as},x}, 0, -\tau J_{\mathrm{s},xy}). \tag{9b}$$

The full expression of the RKKY components can be found in Appendix; the $J_{x/y/z}$ couplings represent the XYZ-Heisenberg interaction, while $J_{\mathrm{s},xy}$ and $J_{\mathrm{as},x/y}$ correspond to the symmetric and Dzyaloshinskii–Moriya (DM) asymmetric interaction, respectively [31].

3. Results and discussion

It is worth noting that our band model and spin susceptibility (normalized by a factor of 10^{-5}) are limited to energies between $-n$ and n which is important for meeting the criterion of meaningful separation of Dirac cones. On the other hand, our theory is valid for all directions φ_R and impurity separations R. From Eq. (A.1), it is evident that $H_{\mathrm{RKKY}}(\varphi_R) = H_{\mathrm{RKKY}}(\varphi_R + m\pi)$, where m is an integer number. Focusing on the in-plane direction of $\varphi_R = \pi/3$, to keep the system stable mechanically and phenomenologically, we set the upper limit of strain modulus to $\pm 10\%$, where $u > 0$ $(u < 0)$ stands for the tensile (compressive) strain. Lastly, we comment that all RKKY components are even under $\Delta_z \to -\Delta_z$.

It is necessary to note that the paper only considers two magnetic impurities residing on the same sublattices TeTe. For the impurities on the same sublattices SnSn, the components $J_{\mathrm{s},xy}$ and $J_{\mathrm{as},y}$ switch their signs for the FM/AFM and clockwise/counterclockwise (CW/CCW) couplings, following Eqs. (8) and (9). Lastly, we note that for the impurities on different sublattices, the components J_y and J_z in the Heisenberg coupling as well as J_x and $J_{\mathrm{s},xy}$ in the DM coupling switch their signs.

In Fig. 2, it is shown how the RKKY couplings behave for different scenarios (when the chemical potential is inside and outside the induced gap) as a function of the impurity separation. The effects of a uniform biaxial strain $u_{xx} = u_{yy} = \pm 5\%$ and the induced gap are considered simultaneously. The results indicate that, for long impurity separations $R/a > 40$, the couplings approach zero due to small values of modified Bessel functions and the competition between the gap and chemical potential, which tunes the available states in the system for RKKY responses. However, oscillations appear for short and intermediate separations, which are responsible for characterizing the FM and AFM couplings depending on the RKKY component. The J_x, J_y, J_z, $J_{\mathrm{s},xy}$, $J_{\mathrm{as},x}$, and $J_{\mathrm{as},y}$ components display AFM, FM, FM, AFM, CCW, and CW couplings between magnetic impurities, respectively, when $\Delta_z < \mu$, i.e., when the chemical potential is outside the gap. When the chemical potential is inside the gap, i.e. $\Delta_z > \mu$, it is observed that the $J_{\mathrm{as},x}$ and $J_{\mathrm{as},y}$ couplings disappear. This is because there are no states in the gap that are involved in the response. As a result, a Heaviside step function can be defined for the asymmetric DM interaction to emphasize that it requires doping. This requirement has been confirmed both theoretically and experimentally in previous studies [31,42]. This can be understood from Eqs. (A.1e) and (A.1f) in which the imaginary of integral vanishes for $\Delta_z > \mu$. For the biaxial strain $u_{xx} = \pm 5\%$ and $u_{yy} = \mp 5\%$, i.e., when the strain components are applied along different directions (compressive/tensile or tensile/compressive), we have $J_{\ell}(\pm u_{xx}, \mp u_{yy}) = -J_{\ell}(\pm u_{xx}, \pm u_{yy})$.

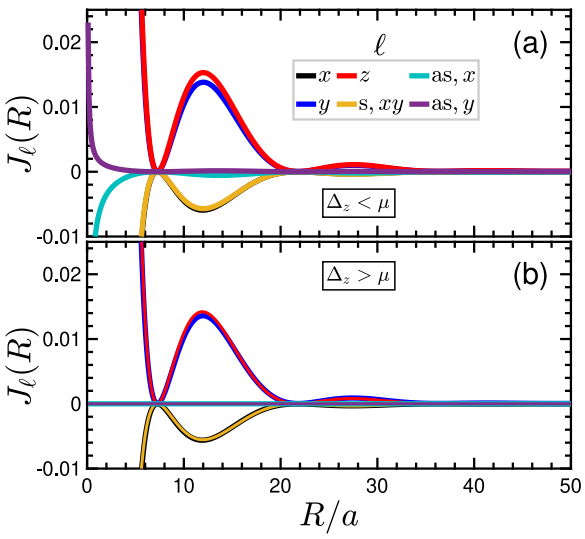

Fig. 2. The behavior of the RKKY couplings on the SnTe(001) surface with respect to the impurity separation R/a along the direction $\varphi_R = \pi/3$, strain $u_{xx/yy} = \pm 5\%$, a chemical potential $\mu = n/2$, and induced gap (a) $\Delta_z = n/4$ and (b) $\Delta_z = n$. The results show that the asymmetric DM components are active only when $\Delta_z < \mu$, while the symmetric and Heisenberg components remain almost unchanged in both regimes $\Delta_z < \mu$ and $\Delta_z > \mu$.

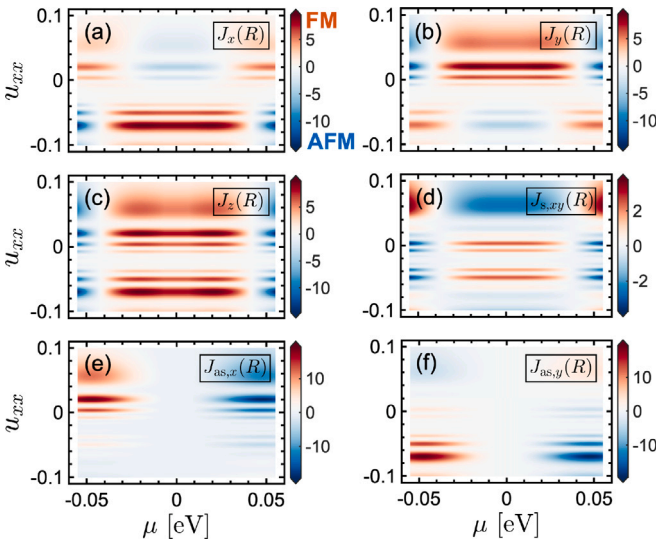

Fig. 3. The RKKY couplings as a function of the chemical potential and biaxial strain (including $u_{yy} = +5\%$) at the impurity separation $R/a = 10$ along the direction $\varphi_R = \pi/3$. The induced gap is $\Delta_z = n/4$. Various switching of FM/AFM and CW/CCW couplings are evident due to the interplay between doping, strain, and gating effects.

Depending on the biaxial strain strength (considering $u_{yy} = +5\%$) and doping in a certain gap strength $\Delta_z = n/4$, different responses can be extracted. Redistribution between the host states involved in the RKKY response via the chemical potential indicates an interesting magnetic moment flipping. The main observation is that the results of the DM components are consistent with the previous finding such that asymmetrical $J_{\mathrm{as},x}$ and $J_{\mathrm{as},y}$ components vanish for $\mu < \Delta_z$ independent of the strain strength, see Figs. 3(e) and 3(f). Additionally, we find $J_{\mathrm{as},x/y}(-\mu) = -J_{\mathrm{as},x/y}(+\mu)$, in agreement with Refs. [31,42], while for Heisenberg and symmetric components, we have $J_{x/y/xy}(-\mu) = +J_{x/y/xy}(+\mu)$, see Figs. 3(a)–(d). For all components, however, the translational symmetry for the strain field $(\vec{u} \to -\vec{u})$ is broken. Interestingly, various switching between FM to AFM couplings occurs, which is the main aim of the present research. For $u_{yy} = -5\%$, we

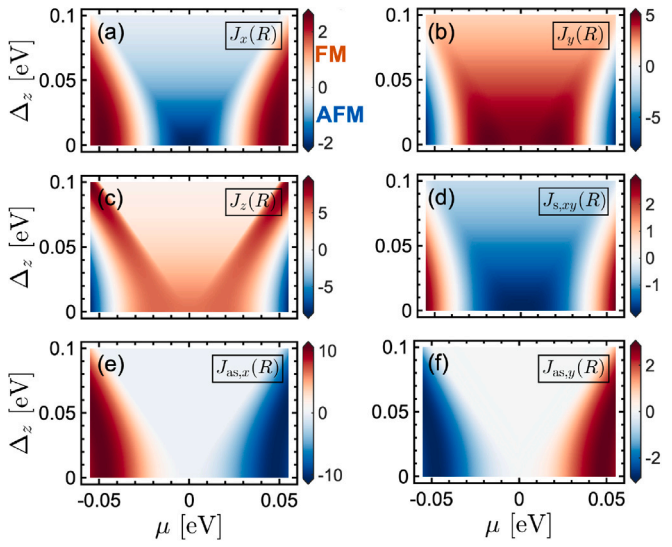

Fig. 4. The RKKY couplings as a function of induced gap and the chemical potential at a biaxial strain of $u_{xx} = \pm 5\%$ and $u_{yy} = \pm 5\%$, with an impurity separation of $R/a = 10$, and the direction $\varphi_R = \pi/3$, it is observed that FM/AFM and CW/CCW couplings do not switch for $\Delta_z > \mu$. These findings shed light on the complex nature of RKKY couplings and the importance of considering multiple factors when analyzing their behavior.

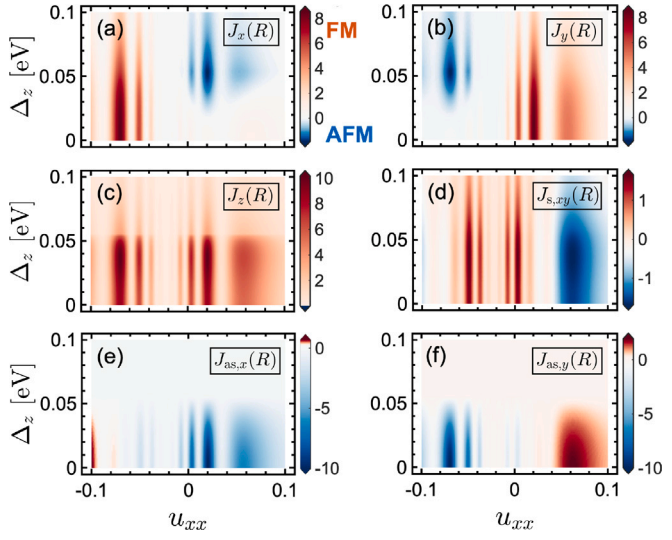

Fig. 5. The RKKY couplings between the two magnetic impurities are analyzed in the presence of different induced gaps and strains at specific conditions. At $u_{yy} = +5\%$, the chemical potential $\mu = n/2$, the impurity separation $R/a = 10$, and the direction $\varphi_R = \pi/3$, the analysis revealed that the gap and strain did not affect the FM coupling of the z-component of the RKKY interaction. However, the study finds various FM/AFM and CW/CCW couplings for other components, indicating the complexity of the interplay between different fields and the rich physics of spintronic applications.

again find the previous relation $J_\ell(\pm u_{xx}, \mp u_{yy}) = -J_\ell(\pm u_{xx}, \pm u_{yy})$. The overall achievement of the study is the ability to control magnetic orderings FM/AFM and CW/CCW in a doped-strained-gapped phase of the SnTe (001) surface, which was previously not well-documented in the literature of RKKY physics in Dirac materials. This finding proposes significant advances in spintronics compared to the pristine phase of matter.

Next, in Fig. 4, we turn to the role of coexisted gap and doping at fixed $u_{xx} = \pm 5\%$, $u_{yy} = \pm 5\%$ with the same set of parameters $R/a = 10$ and $\varphi_R = \pi/3$. As we discussed before, the RKKY interaction vanishes for asymmetric DM components for $\mu < \Delta_z$. It is also the case for $-\mu > \Delta_z$, i.e., $J_{as,x/y} = 0$ for $|\mu| < \Delta_z$, as presented in Figs. 4(e) and 4(f). In addition to the relation $J_{as,x/y}(-\mu) = J_{as,x/y}(\mu)$, we observe the following relation $J_{as,y/x}(-\mu) = -J_{as,x/y}(\mu)$. The susceptibility in Eqs. (A.1a)–(A.1d) is directly related to the physics of the system. Upon careful consideration, it appears that the final response of the susceptibility is determined by the competition between the chemical potential and the induced gap. It turns out that the Heisenberg and symmetric components switch their initial FM and AFM couplings only when $|\mu| > \Delta_z$, as shown in Figs. 4(a)–(d). Interestingly, this behavior is independent of the gap size. By analyzing the spatial symmetries in the strained model, it is found that

$$J_{x/y/z}(\pm u_{xx}, \mp u_{yy}) = J_{y/x/z}(\pm u_{xx}, \pm u_{yy}), \tag{10a}$$

$$J_{s,xy}(\pm u_{xx}, \mp u_{yy}) = -J_{s,xy}(\pm u_{xx}, \mp u_{yy}), \tag{10b}$$

$$J_{as,x}(\pm u_{xx}, \mp u_{yy}) = J_{as,x}(\pm u_{xx}, \mp u_{yy}), \tag{10c}$$

$$J_{as,y}(\pm u_{xx}, \mp u_{yy}) = -J_{as,y}(\pm u_{xx}, \mp u_{yy}). \tag{10d}$$

Now, we focus on the competition between the gap and strain in tuning or switching the FM/AFM and CW/CCW couplings, as shown in Fig. 5. This configuration is presented for pedagogical and comprehensive purposes to further our understanding of the interplay between gap, strain, and magnetic couplings in TCIs. First, we argue that for a fixed $u_{yy} = +5\%$ and $\mu = n/2$, all RKKY components behave as $J_\ell(-u_{yy}) = -J_\ell(+u_{yy})$. In this phase, the asymmetrical treatments mentioned before hold for the strain dependencies. For $\Delta_z \geq 0.055$ eV, i.e., for $\Delta_z > 2\mu$, J_z and DM couplings approach zero. In contrast to the two previous systematic investigations in Figs. 3 and 4, there is no FM and AFM switching between magnetic moments of impurities for the J_z component, while both FM/AFM and CW/CCW couplings can appear for the other five components. To mimic the sensitivity to the gap and strain in the experiment, a gate along with applying the ferroelectric distortion to control the low-energy orientations has been applied, as reported in previous studies [35,43]. These techniques can ultimately be linked to the RKKY interaction on the surface of TCIs in the way we proposed here.

4. Conclusions

Assessing the magnetic structure of topological materials that have strong spin–orbit coupling due to the presence of heavy atoms in their compounds, is challenging to do so because their surface density of states is high. However, we used real-space Green's function and linear response theory techniques to reveal the evolution of ferromagnetic (FM) and antiferromagnetic (AFM) couplings as well as clockwise (CW) and counterclockwise (CCW) between two magnetic impurities on the doped, strained, and gapped (001) surface of a topological crystalline insulator SnTe. We also derived the FM-AFM and CW-CCW phase diagrams of this compound in the low-energy limit, which was previously unknown. We argue that the magnetic cross-talk between impurities on the SnTe(001) surface can be differently impacted by various electrical and mechanical fields. Therefore, the interplay between them should be fully accounted for in reality when their rich physics is considered for spintronic applications.

CRediT authorship contribution statement

Bui D. Hoi: Writing – review & editing, Writing – original draft, Validation, Software, Methodology, Investigation, Funding acquisition, Formal analysis, Data curation, Conceptualization. **Doan Q. Khoa:** Writing – original draft, Validation, Software, Investigation, Data curation, Conceptualization. **Nguyen T. Dung:** Writing – original draft, Visualization, Validation, Investigation, Data curation, Conceptualization. **Ho Viet:** Visualization, Validation, Software, Investigation, Data curation. **Vo T. Lam:** Writing – original draft, Validation, Investigation, Formal analysis, Data curation, Conceptualization.

Declaration of competing interest

The authors declare that they have no known competing financial interests or personal relationships that could have appeared to influence the work reported in this paper.

Data availability

Data will be made available on request.

Acknowledgments

This research is funded by Vietnam National Foundation for Science and Technology Development (NAFOSTED) under grant number 103.01-2021.68.

Appendix. RKKY components

By defining $J_\ell(\vec{R}) = \tilde{J}_\ell(\vec{R})/\pi\mathcal{J}^2\mathcal{C}^2$, we have

$$\tilde{J}_x(\vec{R}) = \pi\mathcal{J}^2\mathcal{C}^2\xi(\vec{R})\Im\int_{o^+}^{\infty} i\,d\varepsilon\,\tilde{\varepsilon}^2\left[K_0^2(\tilde{\varepsilon}\,R/v_F) + \cos(2\tilde{\varphi}_R)K_1^2(\tilde{\varepsilon}\,R/v_F)\right], \quad \text{(A.1a)}$$

$$\tilde{J}_y(\vec{R}) = \pi\mathcal{J}^2\mathcal{C}^2\xi(\vec{R})\Im\int_{o^+}^{\infty} i\,d\varepsilon\,\tilde{\varepsilon}^2\left[K_0^2(\tilde{\varepsilon}\,R/v_F) - \cos(2\tilde{\varphi}_R)K_1^2(\tilde{\varepsilon}\,R/v_F)\right], \quad \text{(A.1b)}$$

$$\tilde{J}_z(\vec{R}) = \pi\mathcal{J}^2\mathcal{C}^2\xi(\vec{R})\Im\int_{o^+}^{\infty} i\,d\varepsilon\,\tilde{\varepsilon}^2\left[K_0^2(\tilde{\varepsilon}\,R/v_F) + K_1^2(\tilde{\varepsilon}\,R/v_F)\right] - \frac{\pi\mathcal{J}^2\mathcal{C}^2\Delta_z^2}{2}\xi(\vec{R})\Im\int_{o^+}^{\infty} i\,d\varepsilon K_0^2(\tilde{\varepsilon}\,R/v_F), \quad \text{(A.1c)}$$

$$\tilde{J}_{s,xy}(\vec{R}) = \pi\mathcal{J}^2\mathcal{C}^2\xi(\vec{R})\Im\int_{o^+}^{\infty} i\,d\varepsilon\,\tilde{\varepsilon}^2\,\sin(2\tilde{\varphi}_R)K_1^2(\tilde{\varepsilon}\,R/v_F), \quad \text{(A.1d)}$$

$$\tilde{J}_{as,x}(\vec{R}) = -2\pi\mathcal{J}^2\mathcal{C}^2\xi(\vec{R})\sin(\tilde{\varphi}_R)\,\Im\int_{o^+}^{\infty} d\varepsilon\,\tilde{\varepsilon}\sqrt{\tilde{\varepsilon}^2 - \Delta_z^2/4}\,\mathbb{K}_0(\tilde{\varepsilon}\,R/v_F)\,\mathbb{K}_1(\tilde{\varepsilon}\,R/v_F), \quad \text{(A.1e)}$$

$$\tilde{J}_{as,y}(\vec{R}) = -2\pi\mathcal{J}^2\mathcal{C}^2\xi(\vec{R})\cos(\tilde{\varphi}_R)\,\Im\int_{o^+}^{\infty} d\varepsilon\,\tilde{\varepsilon}\sqrt{\tilde{\varepsilon}^2 - \Delta_z^2/4}\,\mathbb{K}_0(\tilde{\varepsilon}\,R/v_F)\,\mathbb{K}_1(\tilde{\varepsilon}\,R/v_F), \quad \text{(A.1f)}$$

where the intersection between Dirac cones along all directions on the SnTe(001) surface with the lattice constant $a \approx 6.3$ Å is given by

$$\xi(\vec{R}) = \cos^2(x\tilde{R}_x) + \cos^2(y\tilde{R}_y) + 2\cos(x\tilde{R}_x)\cos(y\tilde{R}_y)\cos\left(\frac{\pi}{\sqrt{2}a}[\tilde{R}_x - \tilde{R}_y]\right), \quad \text{(A.2)}$$

where $\tilde{R}_x = R\cos(\tilde{\varphi}_R)$ and $\tilde{R}_y = R\sin(\tilde{\varphi}_R)$.

References

[1] I. Radu, K. Vahaplar, C. Stamm, T. Kachel, N. Pontius, H.A. Dürr, T.A. Ostler, J. Barker, R.F.L. Evans, R.W. Chantrell, A. Tsukamoto, A. Itoh, A. Kirilyuk, T. Rasing, A.V. Kimel, Transient ferromagnetic-like state mediating ultrafast reversal of antiferromagnetically coupled spins, Nature 472 (7342) (2011) 205–208.

[2] J.H. Mentink, J. Hellsvik, D.V. Afanasiev, B.A. Ivanov, A. Kirilyuk, A.V. Kimel, O. Eriksson, M.I. Katsnelson, T. Rasing, Ultrafast spin dynamics in multisublattice magnets, Phys. Rev. Lett. 108 (2012) 057202.

[3] R.F.L. Evans, T.A. Ostler, R.W. Chantrell, I. Radu, T. Rasing, Ultrafast thermally induced magnetic switching in synthetic ferrimagnets, Appl. Phys. Lett. 104 (8) (2014) 082410.

[4] D.D. Awschalom, M.E. Flatté, Challenges for semiconductor spintronics, Nat. Phys. 3 (3) (2007) 153–159.

[5] R. Hanson, L.P. Kouwenhoven, J.R. Petta, S. Tarucha, L.M.K. Vandersypen, Spins in few-electron quantum dots, Rev. Modern Phys. 79 (2007) 1217–1265.

[6] T. Kasuya, A Theory of Metallic Ferro- and Antiferromagnetism on Zener's Model, Progr. Theoret. Phys. 16 (1) (1956) 45–57.

[7] K. Yosida, Magnetic properties of Cu-Mn alloys, Phys. Rev. 106 (1957) 893–898.

[8] M.A. Ruderman, C. Kittel, Indirect exchange coupling of nuclear magnetic moments by conduction electrons, Phys. Rev. 96 (1954) 99–102.

[9] C. Kittel, Indirect exchange interactions in metals**supported by the national science foundation, in: F. Seitz, D. Turnbull, H. Ehrenreich (Eds.), in: Solid State Physics, vol. 22, Academic Press, 1969, pp. 1–26.

[10] S. Saremi, RKKY in half-filled bipartite lattices: Graphene as an example, Phys. Rev. B 76 (2007) 184430.

[11] A.M. Black-Schaffer, RKKY coupling in graphene, Phys. Rev. B 81 (2010) 205416.

[12] M. Sherafati, S. Satpathy, RKKY interaction in graphene from the lattice Green's function, Phys. Rev. B 83 (2011) 165425.

[13] M. Sherafati, S. Satpathy, Analytical expression for the RKKY interaction in doped graphene, Phys. Rev. B 84 (2011) 125416.

[14] V.K. Dugaev, V.I. Litvinov, J. Barnas, Exchange interaction of magnetic impurities in graphene, Phys. Rev. B 74 (2006) 224438.

[15] O. Roslyak, G. Gumbs, D. Huang, Gap-modulated doping effects on indirect exchange interaction between magnetic impurities in graphene, J. Appl. Phys. 113 (12) (2013) 123702.

[16] H. Zhang, C.-X. Liu, X.-L. Qi, X. Dai, Z. Fang, S.-C. Zhang, Topological insulators in Bi_2Se_3, Bi_2Te_3 and Sb_2Te_3 with a single Dirac cone on the surface, Nat. Phys. 5 (6) (2009) 438–442.

[17] J.E. Moore, L. Balents, Topological invariants of time-reversal-invariant band structures, Phys. Rev. B 75 (2007) 121306.

[18] A.P. Schnyder, S. Ryu, A. Furusaki, A.W.W. Ludwig, Classification of topological insulators and superconductors in three spatial dimensions, Phys. Rev. B 78 (2008) 195125.

[19] R. Roy, Topological phases and the quantum spin Hall effect in three dimensions, Phys. Rev. B 79 (2009) 195322.

[20] L. Fu, C.L. Kane, E.J. Mele, Topological insulators in three dimensions, Phys. Rev. Lett. 98 (2007) 106803.

[21] R.-J. Slager, A. Mesaros, V. Juričić, J. Zaanen, The space group classification of topological band-insulators, Nat. Phys. 9 (2) (2013) 98–102.

[22] F. Zhang, C.L. Kane, E.J. Mele, Topological mirror superconductivity, Phys. Rev. Lett. 111 (2013) 056403.

[23] W.A. Benalcazar, J.C.Y. Teo, T.L. Hughes, Classification of two-dimensional topological crystalline superconductors and Majorana bound states at disclinations, Phys. Rev. B 89 (2014) 224503.

[24] J.C.Y. Teo, L. Fu, C.L. Kane, Surface states and topological invariants in three-dimensional topological insulators: Application to $Bi_{1-x}Sb_x$, Phys. Rev. B 78 (2008) 045426.

[25] L. Fu, Topological crystalline insulators, Phys. Rev. Lett. 106 (2011) 106802.

[26] T.H. Hsieh, H. Lin, J. Liu, W. Duan, A. Bansil, L. Fu, Topological crystalline insulators in the SnTe material class, Nature Commun. 3 (1) (2012) 982.

[27] Y. Tanaka, Z. Ren, T. Sato, K. Nakayama, S. Souma, T. Takahashi, K. Segawa, Y. Ando, Experimental realization of a topological crystalline insulator in snte, Nat. Phys. 8 (11) (2012) 800–803.

[28] P. Dziawa, et al., Topological crystalline insulator states in $Pb_{1-x}Sn_xSe$, Nature Mater. 11 (12) (2012) 1023–1027.

[29] S.-Y. Xu, et al., Observation of a topological crystalline insulator phase and topological phase transition in $Pb_{1-x}Sn_xTe$, Nature Commun. 3 (1) (2012) 1192.

[30] H. Cheraghchi, M. Yarmohammadi, Anisotropic ferroelectric distortion effects on the RKKY interaction in topological crystalline insulators, Sci. Rep. 11 (1) (2021) 5273.

[31] M. Yarmohammadi, M. Bukov, M.H. Kolodrubetz, Noncollinear twisted RKKY interaction on the optically driven SnTe(001) surface, Phys. Rev. B 107 (2023) 054439.

[32] M. Ameziane, R. Rosenkamp, L. Flajšman, S. van Dijken, R. Mansell, Electric field control of RKKY coupling through solid-state ionics, Appl. Phys. Lett. 122 (23) (2023) 232401.

[33] J. Liu, W. Duan, L. Fu, Two types of surface states in topological crystalline insulators, Phys. Rev. B 88 (2013) 241303.

[34] M. Ezawa, Valleytronics on the surface of a topological crystalline insulator: Elliptic dichroism and valley-selective optical pumping, Phys. Rev. B 89 (2014) 195413.

[35] M. Serbyn, L. Fu, Symmetry breaking and Landau quantization in topological crystalline insulators, Phys. Rev. B 90 (2014) 035402.

[36] M. Yarmohammadi, H. Cheraghchi, Effective low-energy RKKY interaction in doped topological crystalline insulators, Phys. Rev. B 102 (2020) 075411.

[37] Y. Okada, et al., Observation of Dirac node formation and mass acquisition in a topological crystalline insulator, Science 341 (6153) (2013) 1496–1499.

[38] D. Walkup, B.A. Assaf, K.L. Scipioni, R. Sankar, F. Chou, G. Chang, H. Lin, I. Zeljkovic, V. Madhavan, Interplay of orbital effects and nanoscale strain in topological crystalline insulators, Nature Commun. 9 (1) (2018) 1550.

[39] B.D. Hoi, Switching of the RKKY coupling on a topological crystalline insulating surface, Phys. Rev. B 109 (2024) 184441.

[40] E. Tang, L. Fu, Strain-induced partially flat band, helical snake states and interface superconductivity in topological crystalline insulators, Nat. Phys. 10 (12) (2014) 964–969.

[41] E. Kogan, RKKY interaction in gapped or doped graphene, Graphene 2 (2013) 8.

[42] C. Liu, Y. Zang, W. Ruan, Y. Gong, K. He, X. Ma, Q.-K. Xue, Y. Wang, Dimensional crossover-induced topological Hall Effect in a magnetic topological insulator, Phys. Rev. Lett. 119 (2017) 176809.

[43] S. Reja, H.A. Fertig, L. Brey, S. Zhang, Surface magnetism in topological crystalline insulators, Phys. Rev. B 96 (2017) 201111.